ISSN 1674-1056
http://cpb.iphy.ac.cn
http://iopscience.iop.org/cpb
中国物理 B
Chinese Physics
中国物理
Chinese Physics B

Surface plasmon polariton nanolasers: Coherent light sources for new applications

Yu-Hsun Chou(周昱薰)), Chia-Jui Chang(張家睿), Tzy-Rong Lin(林資榕), Tien-Chang Lu(盧廷昌)

Citation: Chin. Phys. B . 2018, 27(11): 114208. **doi:** 10.1088/1674-1056/27/11/114208

Journal homepage: http://cpb.iphy.ac.cn; http://iopscience.iop.org/cpb

What follows is a list of articles you may be interested in

Surface plasmon polariton waveguides with subwavelength confinement

Longkun Yang(杨龙坤), Pan Li(李盼), Hancong Wang(汪涵聪), Zhipeng Li(李志鹏)

Chin. Phys. B . 2018, 27(9): 094216. **doi:** 10.1088/1674-1056/27/9/094216

Plasmonically induced reflection in metal-insulator-metal waveguides with two silver baffles coupled square ring resonator

Zhi-Dong Zhang(张志东), Lian-Jun Ma(马连俊), Fei Gao(高飞), Yan-Jun Zhang(张彦军), Jun Tang(唐军), Hui-Liang Cao(曹慧亮), Bin-Zhen Zhang(张斌珍), Ji-Cheng Wang(王继成), Shu-Bin Yan(闫树斌), Chen-Yang Xue(薛晨阳)

Chin. Phys. B . 2017, 26(12): 124212. **doi:** 10.1088/1674-1056/26/12/124212

A novel phase-sensitive scanning near-field optical microscope

Wu Xiao-Yu, Sun Lin, Tan Qiao-Feng, Wang Jia

Chin. Phys. B . 2015, 24(5): 054204. **doi:** 10.1088/1674-1056/24/5/054204

Transmission through array of subwavelength metallic slits curved with a single step or multi-step

Wang Ying-Qi, Wang Yan-Hua, Zheng Xian-Hua, Ye Jia-Sheng, Zhang Yan, Liu Shu-Tian

Chin. Phys. B . 2014, 23(3): 034202. **doi:** 10.1088/1674-1056/23/3/034202

Infrared emissivities of Mn, Co co-doped ZnO powders

Yao Yin-Hua, Cao Quan-Xi

Chin. Phys. B . 2012, 21(12): 124205. **doi:** 10.1088/1674-1056/21/12/124205

TOPICAL REVIEW — Nanolasers

Surface plasmon polariton nanolasers: Coherent light sources for new applications*

Yu-Hsun Chou(周昱薰)[1], Chia-Jui Chang(張家睿)[2], Tzy-Rong Lin(林資榕)[3,4], and Tien-Chang Lu(盧廷昌)[2,†]

[1] *Physics Department, University of Michigan, 450 Church Street, Ann Arbor, MI 481092-122, USA*
[2] *Department of Photonics, "National" Chiao Tung University, Hsinchu 300, Taiwan, China*
[3] *Department of Mechanical and Mechatronic Engineering, "National" Taiwan Ocean University, Keelung 20224, Taiwan, China*
[4] *Center of Excellence for Ocean Engineering, "National" Taiwan Ocean University, Keelung 20224, Taiwan, China*

(Received 28 February 2018; revised manuscript received 15 June 2018; published online 25 October 2018)

The invention of the Internet and mobile devices has caused tremendous changes in human lives over the past two decades. Information technology has broken through limitations of geospatial space, enabling extremely high-speed data transmission and new types of data services. In recent years, demands for data processing have shown an increasing trend. Furthermore, data generated from internet-related applications such as cloud services and self-driving technology are likely to grow exponentially over the coming years. Currently, data transmission inside integrated circuits mainly relies on metal wires. However, the substantial resistive–capacitive delay and energy loss that are caused by metal wires limit data transmission speeds. Optical interconnection has been regarded as a major solution to efficiently reduce energy consumption and increase data transmission speeds. The size of conventional semiconductor laser devices, which are the key component in optical interconnection, cannot be smaller than the wavelength of light, which is a fundamental physical obstacle to lasers integrating with current electronic integrated circuits in reasonable volumes. To realize optical interconnection, the volume of the laser device must match the existing electronic components. Recently, the use of diffraction-unlimited plasmonic lasers has been successfully demonstrated, and these have great potential in different applications. In this paper, we discuss the recent progress toward surface plasmon polariton lasers and provide practical insights into the challenges in realizing these novel devices.

Keywords: ZnO, surface plasmon polariton, silver, laser

PACS: 42.55.Px **DOI:** 10.1088/1674-1056/27/11/114208

1. Introduction

1.1. Limitations of laser downscaling

The first laser was invented by Maiman in 1960, and efforts to downsize lasers have continued ever since, as indicated in Fig. 1.[1] The first breakthrough in the reduction of lasers came with the invention of the semiconductor laser in 1962, which enabled lasers to be reduced from several meters to only a few hundred micrometers.[2] In 1979, Iga *et al.* demonstrated the world's first vertical cavity surface-emitting laser (VCSEL), which reduced the size of lasers to tens of microns.[3] The invention of the VCSEL opened the door for on-chip optical interconnection. Although the size of lasers can be further scaled down to a few microns by utilizing microstructures such as microdisks/spheres,[4,5] defect-type photonic crystals,[6] and semiconductor nanowires,[7] the cavity size remains in the order of several $(\lambda/n)^3$, where n is the refractive index of the cavity.

The main challenge of shrinking down the scale of a laser cavity is the fundamental diffraction law in optics, which restricts the size of a laser to half of the wavelength. An effective method to miniaturize the volume of semiconductor lasers into the subwavelength scale is to concentrate the field of the photonic mode inside a metal-clad cavity.[8–13] However, the loss of the noble metal is high, and the development of metal-clad semiconductor laser devices is restricted for near-infrared (NIR) applications. As an alternative, Bergman and Stockman theoretically proposed a novel device with a plasmonic nanoresonator surrounded by gain media, surface plasmon (SP)-based amplification of stimulated emission of radiation (spaser), which can generate a strongly localized coherent SP mode in a subwavelength scale.[14–16] Inspired by this concept, the first spaser was demonstrated by Noginov *et al.* in 2009.[17] However, the realization of spasing required a well-controlled and delicate laboratory environment.[18] Instead of utilizing the localized SP effect for the feedback mechanism, Hill *et al.* demonstrated a new class of laser based on an metal–insulator–semiconductor–insulator–metal structure with the cavity width half the diffraction limit; this was the first SP mode laser in the NIR region.[19] Meanwhile, Oulton *et al.* demonstrated a simpler SP mode laser based on a semiconductor–insulator–metal (SIM) structure that ex-

*Project supported by Grant Nos. MOST 1042221E009096MY3, MOST 1042923E009003MY3, MOST 1032221E019028MY3, MOST 1062917I564021, and MOST 1052221E019049MY3.
†Corresponding author. E-mail: timtclu@mail.nctu.edu.tw
© 2018 Chinese Physical Society and IOP Publishing Ltd

ploited the interaction between the SP polariton (SPP) and gain media.[20] Although the mode area of their laser can be as small as $\lambda^2/400$, the length of the nanowire remains in the scale of a few microns.

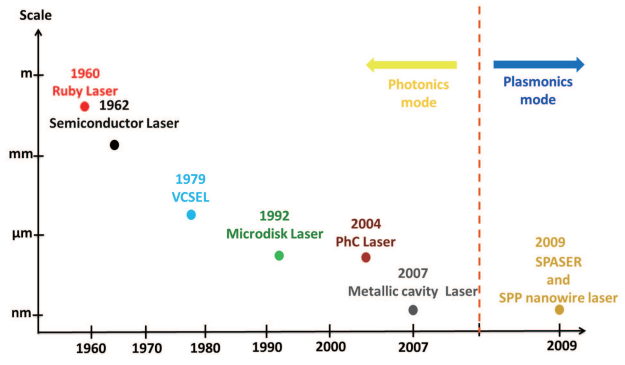


Fig. 1. (color online) Miniaturization progress of semiconductor laser size.[1–8]

By improving the metal quality to reduce damping losses and combining with a high-quality GaN/InGaN core shell nanorod, Lu *et al.* demonstrated the first continuous-wave (CW) operation plasmonic nanolaser with a subwavelength scale in all three dimensions; this was the first diffraction-unlimited SPP laser.[21] Later, they demonstrated single-mode plasmonic nanolaser emission with the full visible spectrum by changing the composition of indium.[22] However, the SPP laser demonstrated by Lu *et al.* can only operate by photon injection, and the operation temperature cannot be higher than 120 K, which is not practical for integration with current devices. To date, a diffraction-unlimited SPP nanolaser with a low lasing threshold, room temperature operation, and electrical pumping has not been demonstrated yet. Improvements in cavity Q-factor, material gain, heat dissipation, and electrical contacts with low resistivity are all required to develop a practical SPP nanolaser.

1.2. Purcell effect

In 1946, Purcell discovered that spontaneous emission is affected by the quality factor (Q) and mode volume (V_{m}) of the cavity. The Purcell factor $F_{\mathrm{P}} = \frac{3}{4\pi^2}\left(\frac{\lambda_{\mathrm{c}}}{n}\right)^3 \frac{Q}{V_{\mathrm{m}}}$ represents the spontaneous emission rate enhancement of the fluorescent molecule by its cavity.[23] Notably, the Purcell factor illustrates that the interaction is independent of the properties of the fluorescent molecule but related to the cavity's properties, which reveals some simple strategies that can be employed to increase the light–matter interaction: increase the quality factor Q or reduce the mode volume V_{m}. Because the size reduction of a laser cavity is related to the enhancement of the Purcell effect, notable research efforts have been made to optimize the cavity geometry for a strong Purcell effect, including studies on micropillars, whispering-gallery mode cavities, defect-type photonic crystal cavities, and microspheres.[24–27] However, the mode volume of optical cavities is diffraction-limited and restricts possibilities to shrink the size of optical cavities to the nanoscale. To overcome the physical limitations of optical diffraction, scientists have recently introduced the concept of metallic nanostructures,[8,15,19] where the mode volume can be further shrunk to the deep subwavelength scale, and the Purcell effect can be strongly enhanced in this scenario. However, a poor Q value is the price for using plasmonic nanostructures, which require special treatments for laser operation.[8–13] In the following section, we discuss the characteristics of both optical cavity and plasmonic lasers.

2. Photonic mode nanolasers

2.1. Photonic crystal laser

A photonic crystal is an artificial periodic dielectric structure that possesses a photonic band gap and was first demonstrated by Yablonovitch in 1987.[28] The electromagnetic wave with frequency in the range of the photonic band gap is forbidden, and it can be used as a laser cavity.[29–34] Photonic crystal lasers can be classified into two types: the photonic crystal band edge laser and the photonic crystal defect laser. The amplified mechanism of a photonic crystal band edge laser relies on a multidirectional distributed feedback effect near the band edges in a large photonic structure, which has potential for high-power and single-mode surface-emitting lasers.[35–44] By contrast, it is possible to create defects on the center of a photonic crystal to confine light with a smaller mode volume and stronger Purcell effect. However, both methods require large numbers of photonic lattice to fulfill the required photonic effect. Typically, the scale of photonic crystal lasers is in the order of tens of microns in the in-plane direction. Although the mode volume of defect-type photonic crystal lasers has been reported to be as small as a few hundred nanometers in diameter, the size of the whole device is still too large to be strictly classified as a nanolaser.[34]

2.2. Semiconductor nanowire laser

Semiconductor nanowires are quasi-one-dimensional structural systems with diameters in the nanoscale. The length of the semiconductor nanowire can range from a few microns to hundreds of microns, constituting a naturally formed optical cavity as well as an optical gain medium.[7,45,46] The large refractive index differences between the nanowire and the environment combined with the epitaxially sharp end facet of the nanowire can serve as a Fabry–Pérot-type laser cavity. Nanowire lasers were developed using the bottom-up method, rather than the traditional top-down fabrication technique.[7] The first room temperature optically pumped semiconductor nanowire laser was demonstrated by Huang *et al.* in a ZnO system.[45] Following their pioneering work, different material-based semiconductor nanowire lasers with different emission wavelengths (from ultraviolet (UV) to NIR) have

been reported.[7] Although semiconductor nanowire lasers have reduced the laser volume to a few $(\lambda_c/n)^3$, they are still diffraction-limited.

2.3. Metallic cavity lasers

An effective approach to scale down the volume of a laser is to confine the optical field inside a nanoscale cavity by using metal as a cover for the surface of the laser cavity.[47] Unlike a traditional dielectric cavity, a metallic cavity has been predicted to show excellent optical field confinement capabilities. It was experimentally reported by Hill *et al.* in 2007, but only operated under 77 K. A thin gold layer with hundreds of nanometers thickness was encapsulated on an InP/InGaAs/InP pillar with a thin Si_3N_4 insulating layer. The metal cladding successfully squeezed the light into a small space with dimensions comparable to the subwavelength scale.[8] Since then, several designs with a metal–dielectric–metal structure have been reported.[8–13] One of the main challenges of using a metallic cavity is the large internal ohmic losses. This is more problematic for a laser device with a small optical gain region. In addition, metallic cavity lasers are typically fabricated through a top-down semiconductor manufacturing process, meaning that the surface roughness of the metal–insulator interface will be induced by the imperfection and cause additional scattering losses. To date, most metallic cavities' quality factors (Q) have been between 100 and 200; nonetheless, the quality factors can be as high as approximately 1000 if they employ a whispering-gallery mode cavity, and room temperature electrically driven laser operation has been successfully demonstrated.[8–13] In general, metal losses are more critical in the short-wavelength region, and all metallic cavity lasers reported have been designed for the NIR wavelength.

3. Plasmonic mode nanolasers

3.1. Concept of spasers

In 1902, Wood observed the abnormal reflection spectrum on a metal grating,[48] and Fano first proposed that this phenomenon is related to the electromagnetic waves that propagate along metal surfaces,[49] which was theoretically described by Hessel and Oliner in 1965.[50] At the same time, Rich found that when a high-energy electron beam passes through a metal thin film, there is an additional energy loss that is related to the interface of the metal thin film.[51] Later in 1968, Rich *et al.* experimentally confirmed the existence of the electromagnetic surface wave by studying the polarized spectrum of the metal grating.[52] In the same year, Kretschmann and Otto demonstrated the excitation of nonradiative surface waves by using the prism-coupling method.[53,54] The surface wave can be described as the collective excitation states of the electrons on the interface between the metal and dielectric; this is known as the SP. SPs can exist at the interface between metals (with a negative real part of the dielectric constant) and a dielectric layer (with a positive real part of the dielectric constant). In discrete nanoscale metallic structures, SPs are strongly confined in a small volume and are known as localized SPs (LSPs). Nonetheless, SPs are quasiparticles with boson features, and they can couple with the excitation electromagnetic wave and form a hybrid state called SPP, as shown in Fig. 3.

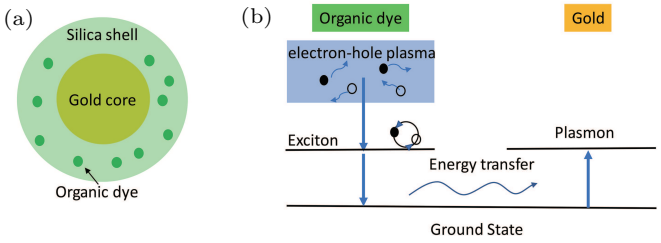


Fig. 2. (color online) (a) Schematic of spaser structure demonstrated by Noginov *et al.* Organic dye provides the optical gain for plasmons generated with Au and stimulates coherent emissions.[17] (b) The spasing model proposed by Stockman.[18] Energy from external excitation generates e–h pairs, which then relax to the exciton level. Excitons with large momentum will transfer their energy to the dark plasmon mode and start the spasing process. The plasmon mode can also couple to the photon mode if the environmental dielectric condition allows. The corresponding photon will carry the same characteristics from the plasmon, resulting in a coherent emission.

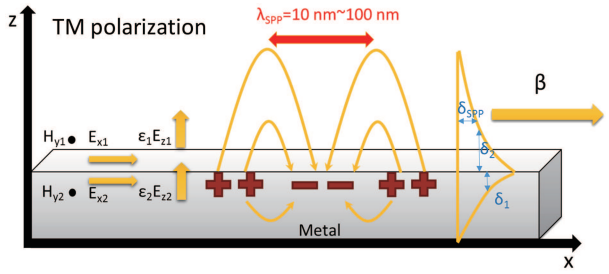


Fig. 3. (color online) Schematic view of an SPP on a metal–dielectric interface. The typical dimension of the SPP wavelength is from 10 nm to 100 nm.

Similar to photons in an optical cavity, SPPs can achieve stimulated emission in a plasmonic cavity. The spaser was first proposed by Bergman and Stockman in 2003. The spaser is similar to a photon laser, and consists of an optical gain medium combined with a plasmonic resonator that can feedback the external excited energy for stimulated coherent SP emission (also known as spasing), as shown in Fig. 2(a). The spasing process can be described as follows: first, an external excitation pumps the gain medium, which transfers the energy to the electron–hole pairs, and they relax to the exciton energy level. The exciton recombines and transfers the energy to the plasmonic resonator, which triggers the stimulated emission of SP, as shown in Fig. 3.[1–16] The stimulated SPs can remain confined as plasmons or they can transfer to the photons by leaving the metallic–dielectric interface. Because the characteristic of the stimulated SP corresponds to the emitted photons, coherence is also observed. Typically, SPs have

a very concentrated electromagnetic field distribution in the subwavelength scale. This unique property allows spasers to have a diffraction-limitless footprint compared with the photon mode nanolaser. Originally, spasers referred to lasers with an LSP feedback mechanism, but a laser dominated by an SPP mode can also be considered a spaser or a more specific SPP laser.

3.2. LSP-based nanolaser

By coating a 14 nm diameter Au nanoparticle with an organic dye-embedded silica shell with a 22 nm outer radius, Noginov *et al.* experimentally demonstrated the first LSP-based nanolaser.[17] In this case, the Au nanoparticle was the plasmonic resonator that supplied feedback for spasing, and Oregon Green 488 dye provided the optical gain that sustained the oscillations on the Au nanoparticle. A narrow spectrum was observed when the pumping power achieved the threshold, demonstrating a clear laser light with a wavelength of 531 nm. This experiment matched the original proposal of the spaser that was based on LSP modes.[14–16] However, single nanoparticle emission was not shown in this experiment; therefore, the possibility of a collective phenomenon cannot be discounted. Nonetheless, Li and Yu noted that a threshold gain of 1.19×10^5 cm^{-1} was required to reach laser operation in this experiment, and such a large threshold gain is due to significant loss resulting from the interband transition of Au nanoparticles at 530 nm.[55] In this case, the threshold gain can only be reduced by manipulating the operation wavelength away from the interband transition region. In 2008, Zheludev *et al.* proposed a two-dimensional asymmetric metallic ring array to support collective in-phase oscillation.[56] Inspired by this concept, Flynn *et al.* demonstrated the first room temperature spasing in 2011 by embedding an Au thin film as a plasmonic waveguide between an InGaAs quantum well.[57] Later, Meng *et al.* experimentally demonstrated a wavelength-tunable spaser by coating a gain material on Au nanorods.[58] Recently, Ramezani *et al.* observed strong light–matter coupling between excitons and LSP coupling in an array of Ag nanoparticles combined with dye molecules.[59] To date, most of the reported spasers have used dye molecules as the optical gain medium to compensate for the metal loss and reduce the size for conducting spasing. However, all studies on LSP-based nanolasers were performed using an ensemble of metallic nanostructures rather than a single one.

3.3. SPP mode nanolasers

Although the original concept of a spaser does not require far-field radiation (photon emission),[14] lasers based on SPP resonators are sometimes loosely categorized as spasers by the research community. In general, spasers are usually associated with localized SP resonators, and SPP lasers are dominated by SPPs. The concept of an SPP laser was first proposed by Oulton *et al.* and Alam *et al.* in 2008,[19,60] and it is based on a Fabry–Pérot plasmonic waveguide with an SIM structure, which can confine the SPs to an extremely small volume, as shown in Fig. 4. However, using the plasmonic waveguide is difficult because of the high losses caused by the metal, which result in a lower quality factor (10–120) compared with that of the dielectric cavity.[20–22,61–65] By optimizing the thickness of the insulating layer and minimizing the losses, Oulton *et al.* demonstrated the first single-device SPP laser by using an SIM waveguide consisting of a single CdS nanowire placed on a silver film with a 5 nm MgF_2 insulating layer. They successfully demonstrated a narrow lasing line and a two-step light in–light out curve, a well-known lasing characteristic. Emissions from two ends of a single nanowire with a diameter below 100 nm were clearly recorded using a beam profiler. Here, the mode area of the fabricated devices is nearly $\lambda^2/400$, and the small mode area leads to a strong Purcell factor of $F_P = 6$.

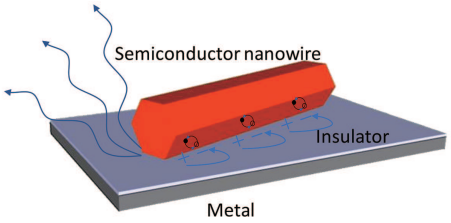


Fig. 4. (color online) Schematic view of an SPP nanolaser with an SIM structure. The well-confined field profile and high momentum of the SPP can couple with the exciton inside the semiconductor. The guided SPP mode can couple to the photon mode at the edge of the nanowire, where the continuum of dielectric condition is broken.

Following this pioneering work, several research efforts based on the SIM structure have been reported with gain medium from the UV to NIR region. Although SIM structures are fascinating with their ability to confine the field to the deep subwavelength scale, most of the demonstrated devices only compress the field to the subwavelength scale in terms of diameter. The scale of the device length is several wavelengths. With the crystal quality improvement caused by InGaN/GaN core shell nanorods (improved exciton performance) placed on an atomic smooth single-crystal silver thin film (lower scattering loss and lower ohmic loss), Lu *et al.* demonstrated the first SPP laser with the field confined to the deep subwavelength scale in all dimensions.[21] By reducing the loss caused by imperfect material quality, they also demonstrated CW operation up to 78 K, a major milestone for fabricating practical devices. Furthermore, they demonstrated a broadband-tunable InGaN/GaN core shell nanorod by changing the ratio of indium in the nanorod.[22] To date, most of the demonstrated Fabry–Pérot-type SPP lasers have suffered from large ohmic and radiation losses, and they have typically exhibited high thresholds (10^1–10^3 MW·cm^{-2}) with operating temperatures lower than 120 K.[20–22] In 2014, Zhang *et*

al. found that a close-contact SIM interface can greatly reduce scattering losses.[62] Within this context, they demonstrated an SPP laser operated at room temperature with an extremely low threshold (3.5 MW·cm^{-2}). In addition to the crystal quality of the metal and semiconductor, the threshold condition and operation temperature also depend on the permittivity combination of the metal and semiconductor. By choosing the appropriate combination of metal and semiconductor, we experimentally demonstrated a single-mode operation and a high operation temperature up to 353 K.[65]

4. Challenges of realizing practical plasmonic mode nanolasers

For practical applications, the following requirements of plasmonic lasers must be fulfilled: (i) minimize metal loss by improving metal quality and optimizing the permittivity combination of the metal and semiconductor; (ii) compensate for the metal loss with high-gain materials; and (iii) develop a suitable device structure for electrical operation.

4.1. Metallic losses and material gain

In general, metal loss is caused by intrinsic metal loss, grain boundary scattering, and surface roughness scattering. Because magnetic interaction is negligible at optical frequencies, permeability is close to unity for commonly used metals. Thus, the optical response of metals can be described by their dielectric permittivity ε.[66] Permittivity is a complex quantity; the real part ε' denotes polarizability, and the imaginary part ε'' relates to energy absorption. Unlike dielectrics, metal has negative real permittivity and nonzero imaginary permittivity at optical frequency.[66] Hence, metal loss is an inherently unavoidable phenomenon that significantly affects the characteristics of SPP lasers. Electrons in metals oscillate with the external electromagnetic field, and each electron affects other electrons in the vicinity. The collective excitation in metals can be described using the Drude model over a wide range of frequency; therefore, the permittivity of the metal has the form[67]

$$\varepsilon(\omega) = \varepsilon_0 - \frac{\varepsilon_0 {\omega_\mathrm{p}}^2}{\omega^2 + \mathrm{i}\gamma\omega},$$

where ε_0 is the vacuum permittivity, ω_p is the plasma frequency of the free electron gas that is proportional to the square root of the concentration of electron gas, and γ denotes the Drude relaxation rate. The aforementioned model indicates that permittivity can only be controlled by reducing the γ or the concentration of electrons at certain frequencies. Typically, noble metals (Au or Ag) are most commonly used for plasmonic devices because of their small ohmic loss.[68] However, the Fermi level in noble metals rises because of filled d band electrons, resulting in a highly polarized background.[69] At optical frequencies, electrons in the valance band or Fermi surface absorb the energy of the photon and transit it to the Fermi surface or conduction band, resulting in significant losses (interband transition). By introducing the background polarization caused by d band electrons, the permittivity for noble metals can be written as follows:

$$\varepsilon(\omega) = \varepsilon_\mathrm{b} - \frac{\omega_\mathrm{p}^2}{\omega^2 + \mathrm{i}\gamma\omega},$$

where ε_b is the background dielectric constant that includes all other polarization contributions in the metal. For Au and Ag, the intraband losses are higher in the longer wavelength and lower in the UV region. By contrast, the interband losses are more notable in the shorter wavelength.[70]

In addition to the intrinsic characteristic of metals, in-plane surface roughness scattering and grain boundaries scattering also decrease the propagation length of the SP and increase the challenge of fabricating low-loss SPP lasers.[71] Typically, metal thin films deposited through evaporation or sputtering possess rough surface and grain boundaries because of polycrystallinity, which reduces the optical characteristics of the devices. The growth process is sensitive to the morphology and surface condition of the substrate, and it is difficult to grow smooth, large-area, and single-crystal metal films on commonly used substrates (e.g. Si, SiO_2, and sapphire).[72,73] Special treatment of the substrate is required to improve the quality of metal thin films.[74–79] Therefore, researchers have begun to develop epitaxial techniques and chemical synthesis for single-crystal growth. By reducing the surface roughness and grain boundaries, researchers have demonstrated a significant reduction in SPP propagation loss.[80–84] We have demonstrated one-dimensional SPP laser operation that exhibited an ultracompact effective mode volume of $V_\mathrm{m} = 1.5 \times 10^{-5}\lambda^3$ and a small group velocity of 1/165 of the speed of light by applying ultrahigh-quality colloidal Ag flakes as the metal layer.[85] In addition to using Au or Ag for plasmonic resonance, epitaxial techniques for single-crystalline Al film growth have shown high potential for realizing practical SPP lasers.[64,65]

Since the first demonstration of a Fabry–Pérot-type SPP laser was realized using a semiconductor nanowire system, several studies on SPP lasing have employed semiconductor materials. To achieve operation at greater than or equal to room temperature, materials such as CdS, GaN, ZnO, and organic–inorganic perovskite that possess large exciton binding energy and oscillator strength are commonly used as the optical gain of SPP lasers.[21,22,62–65] However, SPP propagation through a single interface requires an optical gain of at least 1000–2000 cm^{-2} to compensate for losses.[86,87] Materials with strong oscillation strengths and exciton binding energies greater than room temperature are favorable for demonstrating a more reliable Fabry–Pérot-type SPP laser. Among

the aforementioned semiconductor materials, ZnO possesses an exciton binding energy (60 meV) two times higher than the room temperature thermal energy (25.6 meV), which makes it a suitable material for stable SPP operation at room temperature and above.[88] The first demonstration of a room temperature ZnO SPP laser was reported by Sidipoorus *et al.*[61] Later, we successfully elevated the operational temperature of the SPP laser up to 353 K by using a high-quality single-crystalline Al film with single-crystalline ZnO nanowire.[65]

Metal halide perovskites that enable low-cost bottom-up solution processing are also suitable for SPP lasers.[90,91] Metal halide perovskites are known for their robust exciton properties that can also sustain room temperature thermal energy.[92] Furthermore, metal halide perovskites with different halide compositions exhibit excellent broadband tunability across the visible spectrum.[93] These properties make metal halide a promising material for broadband-tunable SPP lasers.

4.2. Tradeoff between confinement factor and plasmon propagation length

In general, fields of the SP in SIM structures expand to both sides of the insulator and metal interface, resulting in increased losses. An alternative method to reduce loss is to optimize the thickness of the insulating layer. A thicker insulating layer leads to lower metallic losses. However, the fields also become less confined in the waveguide, leading to a weaker coupling between the guide mode and semiconductor nanowire. Conversely, as the thickness of the insulator decreases, the field distribution becomes strongly confined in the gain and metal region, which increases the confinement factor and the modal loss. As analyzed using the finite element method, SIM waveguides possess tradeoffs between the acceptable propagation length and confinement factor. To minimize the threshold, the scaling effect of the SPP laser should be considered.[63,89] Thus, the structural parameters should be carefully designed to optimize the propagation length and confinement factor. Here, the propagation length L_{p} represents the distance that the SP can propagate, which is determined by the imaginary part of the modal propagation constant k_z as $L_{\mathrm{p}} = [2\,\mathrm{Im}(k_z)]^{-1}$. The waveguide confinement factor of the SPP cavity is determined by the ratio of the modal gain to the material gain in the active region, which can be expressed as follows:[94]

$$\Gamma = (n_{\mathrm{a}}/2\eta_0)\int_{A_{\mathrm{a}}} |E(\rho)|^2\,\mathrm{d}\rho/P_z, \tag{1}$$

where n_{a} is the refractive index of the semiconductor nanowire, η_0 is the impedance of metal, $E(\rho)$ is the electric field expressed in cylindrical coordinates, P_z is the power flow along the wire direction, and A_{a} is the area of the gain medium. The transparency threshold gain of the SPP laser should be the gain with which the SPP can propagate along the waveguide without attenuation, which can be expressed as $g_{\mathrm{tr}} = \left(L_{\mathrm{p}}\Gamma_{\mathrm{wg}}\right)^{-1}$. A_{m} is the mode area of the SPP, which indicates the ability of the material gain to amplify a mode extending beyond the semiconductor nanowire to be written as the ratio

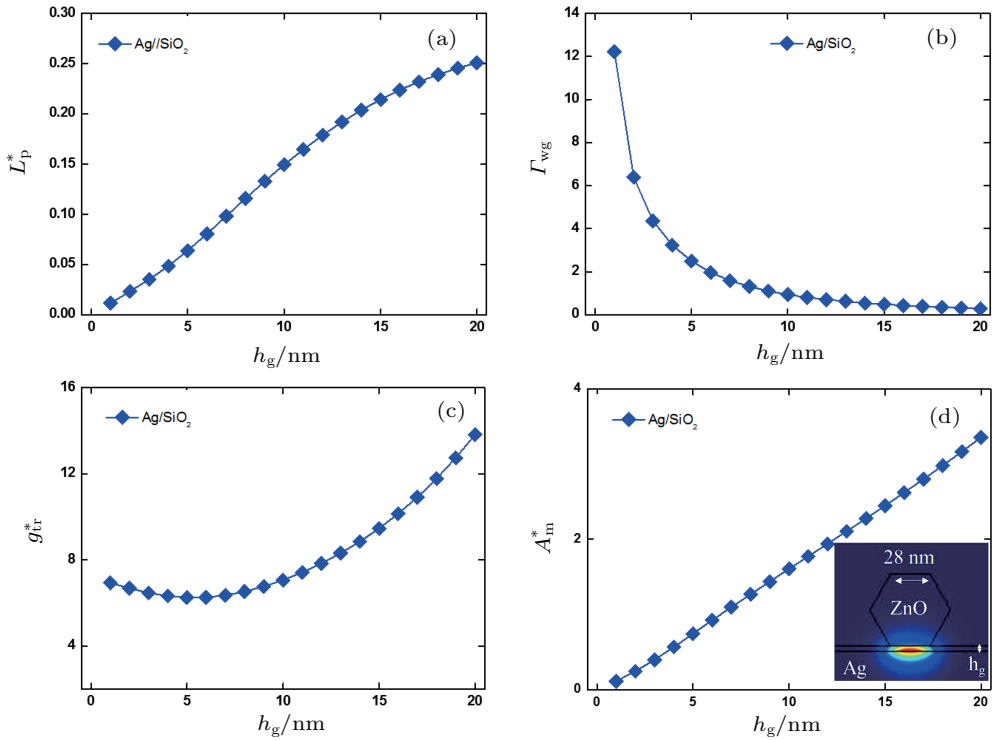


Fig. 5. (color online) Characteristics of SP modes as functions of the insulating layer thickness h_{g}, with a fixed ZnO nanowire side length. (a) Normalized propagation length. (b) Waveguide confinement factor. (c) Normalized transparency threshold gain. (d) Normalized mode area.

of the total mode energy to the peak energy density.[19] Figure 5 shows the propagation length, waveguide confinement factor, transparency gain, and mode area of a ZnO/SiO_2/Ag SPP laser as functions of the insulating layer thickness. L_p^* is the normalized propagation length, which can be express as $L_p^* = L_p/\lambda$. The corresponding normalized transparency threshold gain can be rewritten as $g_{tr}^* = \left(L_p^* \Gamma_{wg}\right)^{-1}$, and the same for the normalized mode area $A_m^* = A_m/\lambda^2$.

Because the coupling between the guided modes of the nanowire and the SPP modes of the metal–insulator interface is stronger with a thinner insulating layer, the confinement of the SPP mode increases as h_g decreases. In addition, the SPP mode field distribution is tightly confined between the metal and gain, which increases the waveguide confinement factor and also reduces the propagation length of SPP, as shown in Fig.s 5(a) and 5(b). By contrast, as the insulating layer increases, the field extends from the waveguide, meaning that the mode area is broader than the laser with thinner h_g, as shown in Fig. 5(d). To fabricate an SPP laser with the lowest transparency threshold gain, the balance between loss and confinement should be optimized by choosing the optimum insulator thickness. ZnO nanowires on Ag films with different insulating layer thicknesses are shown in Fig. 5(c). The plasmonic effect enhances the mode confinement and losses when h_g is small; by contrast, the mode confinement and loss are weak when h_g increases. Thus, laser operation cannot be observed when h_g is too high or too low.

4.3. High-temperature operation

Although SPP lasers have the advantage of compact size, most reported examples were photoexcited and could only be realized at low temperature. Heat might accumulate on a high-density integrated circuit and result in temperatures greater than 30 °C. Therefore, the operation temperature of a practical SPP laser should be higher than room temperature. To realize an SPP laser that can be operated at higher temperatures, several improvements should be considered: (i) increase the metal quality to reduce internal ohmic loss; (ii) reduce the roughness of the metal–dielectric interface for lower scattering loss; (iii) use materials with high exciton binding energy and high oscillation strength as the optical gain medium; and (iv) select materials with the most suitable permittivity combination of the metal and gain medium for generating low-loss SPP waves with a high confinement factor.[95–97] The first to third improvements have been discussed previously. Here, we focus on the fourth improvement. Typically, SPP lasers employ SIM structures to guide the SPP wave within the metal–dielectric interface. The condition for SP propagation through the interface is given by $\varepsilon_d \varepsilon_m < 0$ and $\varepsilon_d + \varepsilon_m < 0$, where ε_d and ε_m represent the permittivity as a function of wavelength.[99] Within this context, the corresponding wavenumber of the SPP mode is inversely proportional to the squared root of permittivity; that is, k_{sp}, $k_y \propto (\varepsilon_m + \varepsilon_d)^{-1/2}$. Because the propagation length and confinement factor of the SPP mode are determined by k_{sp} and k_y, a suitable combination of metal and dielectric will lead to a minimum transparency threshold gain.[65] Through theoretical calculations and experiments, we found that the Al-based ZnO SPP laser has an average threshold density three times lower than that of the Ag-based ZnO SPP laser.[65] According to our calculations, the permittivity combination for Al/ZnO or Al/Al_2O_3 showed no local minima in the ZnO emission energy range, which means that the insulating layer is not necessary for ZnO/Al SPP laser in the near UV–visible wavelength, as shown in Fig. 6(a). According to our calculation, as displayed in Fig. 6(b), the rapidly increasing confinement factor can compensate for the propagation loss as the insulator thickness decreases, which results in the lowest threshold occurring at an insulator thickness of 0. Thus, the Al/ZnO SPP laser has a threshold density two times lower than Al/Al_2O_3/ZnO ($h_g = 5$), as shown in Fig. 6(c). By using single-crystal Al film as the metal layer, ZnO with robust exciton properties as the gain medium, and eliminating the insulating layer, we successfully demonstrated SPP laser operation up to 80 °C.[65]

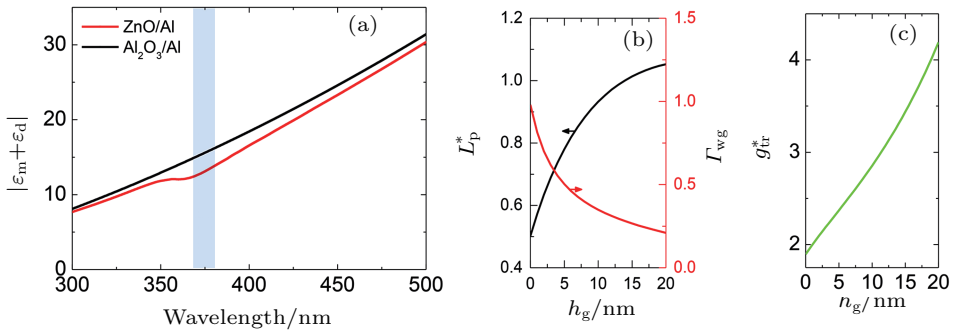


Fig. 6. (color online) (a) The absolute permittivity summation of Al and ZnO as a function of wavelength. The shaded area is the typical exciton emission wavelength from 77 K to 300 K. (b) Normalized propagation length and the confinement factor. (c) Normalized transparency gain. Adapted by permission from the American Chemical Society[65] copyright 2016.

4.4. Electrically pumped nanolasers

Developing an electrically driven CW operation nanolaser is difficult. Although room temperature electrically driven CW nanolasers have already been realized in metal-clad semiconductor cavities (optical mode),[8–13] they have only been possible in the NIR region. This is because surface roughness is difficult to control when applying top-down fabrication methods; moreover, metal losses are lower in the long wavelengths for noble metals. Consequently, most top-down fabricated metal-clad cavities were designed for small band gap materials such as InGaAs or InGaAsP. So far, no report has successfully demonstrated a diffraction-unlimited electrically driven CW SPP nanolaser at room temperature. In principle, a practical SPP laser requires a high Q-factor, small device footprint, favorable thermal dissipation, and low resistance electrical contacts. Although several designs for SPP lasers have been demonstrated in the past decade, these devices are mostly based on the SIM structure that requires an external optical pump to reach the laser operation. The original purpose of the insulating layer in the SIM structure is to reduce loss caused by the metal. However, dielectric materials are not conductive and have poorer thermal conductivity compared with metal, and thus the use of insulating layers limits the design of electrically pumped SPP nanolasers and is detrimental to heat dissipation, especially under high-excitation conditions. In addition, extrinsic scattering loss caused by the rough insulating layer also increases the threshold for SPP nanolasers. Because the insulating layer is unnecessary for the structure of SPP lasers, gain material directly in contact with metal may improve thermal dissipation and conduction efficiency, which provides new possibilities for future SPP laser design.

5. Potential of plasmonic mode nanolasers

5.1. High-speed modulation

The strong Purcell effect inside the SPP cavity enhances the carrier recombination rate, leading to a modulation bandwidth up to the THz scale.[61,63,100] To understand the dynamic characteristics of single-mode SP nanolasers, the gain saturation effect and carrier relaxation time should also be considered. The dynamics of SPP nanolasers can be described by a set of rate equations

$$\frac{\mathrm{d}n_{\mathrm{A}}}{\mathrm{d}t} = \eta\eta' P - \frac{n_{\mathrm{A}}}{\tau_{\mathrm{AB}}}, \tag{2}$$

$$\frac{\mathrm{d}n_{\mathrm{B}}}{\mathrm{d}t} = \frac{n_{\mathrm{A}}}{\tau_{\mathrm{AB}}} - \frac{F}{\tau_{\mathrm{r}}} n_{\mathrm{B}} - F v_{\mathrm{g}} \frac{a(n_{\mathrm{B}} - n_{\mathrm{tr}})}{1+\varepsilon s} s, \tag{3}$$

$$\frac{\mathrm{d}s}{\mathrm{d}t} = \Gamma\beta \frac{F}{\tau_{\mathrm{r}}} n_{\mathrm{B}} + \Gamma F v_{\mathrm{g}} \frac{a(n_{\mathrm{B}} - n_{\mathrm{tr}})}{1+\varepsilon s} s - \gamma s, \tag{4}$$

where n_{A}, n_{B}, and s are the density of reservoir excitons, ground state excitons, and SP, respectively; η is the injection efficiency; η' is the pump in proportion to the excitation power density that can be estimated by the ratio between the nanowire and the spot size of the excitation beam; and P is the nonresonance pump power density. The lifetime of exciton transition from exciton reservoir to ground state is given by τ_{AB}. Here, we only focus on the pumping power below the Mott transition density in which the coupling between the exciton and SPP is not destroyed: τ_{r} is the lifetime of the exciton staying at the ground state, which is strongly enhanced by the small cavity, and the exciton to SPP transition rate is enlarged by the Purcell factor F; $v_{\mathrm{g}} = c/n_{\mathrm{g}}$ is the group velocity of the SP mode inside the cavity; n_{g} is the corresponding group index; a is the differential gain of the semiconductor; n_{tr} is the transparent exciton density of the semiconductor; ε refers to the gain saturation coefficient; and n_{tr} is the transparent exciton density of the semiconductor. When the density of the exciton and SPP increases, the optical gain cannot be maintained at the linear region and begins to saturate. As shown in Fig. 7(a), the relaxation frequency is suppressed by the gain saturation effect. The corresponding small-signal frequency responses for various pumping conditions are shown in Fig. 7(b). At over ten times the threshold pumping power, the frequency response begins to drop off and the resonance peak disappears. Our results indicate an upper limit for the modulation speed of the SPP nanolasers due to the gain saturation effect. However,

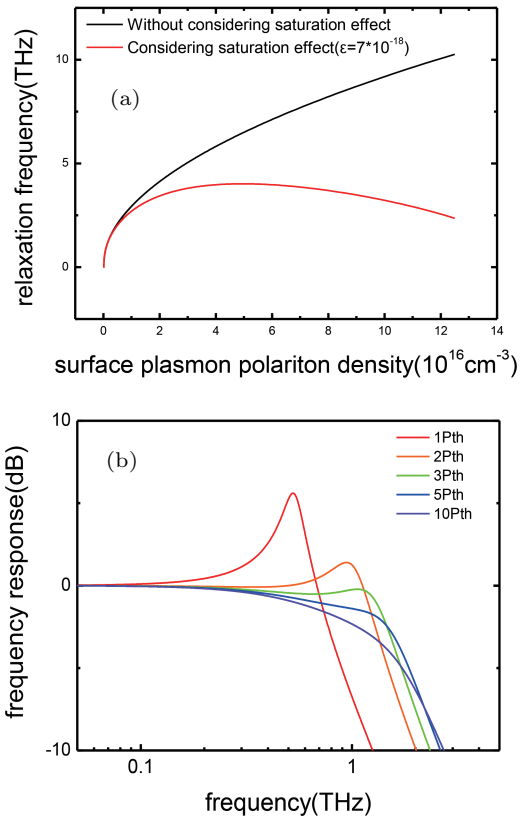


Fig. 7. (color online) (a) Relaxation frequency of SPP nanolasers as a function of SPP density, where the gain saturation effect and exciton relaxation effect were counted. (b) The corresponding frequency response plot.

the modulation speed of the SPP nanolaser is still in the region of a few THz. Such a fast turn-on effect is attributed to the strong Purcell effect that drastically increases the exciton recombination rate and the short cavity lifetime because of the extremely small cavity size. The exhibited modulation performance combined with broadband-tunable materials such as InGaN/GaN core shell nanowire and metal halide perovskite could be applied for use in future on-chip dense wavelength-division multiplexing for high-speed data processing.

5.2. Plasmonic mode nanolaser array

By fabricating subwavelength metal gratings on colloidal Ag flakes, we successfully confined SPs to the edge of a metal grating and demonstrated the operation of an SPP nanolaser array, as shown in Fig. 8.[85] In this structure, the modal volume of the surface plasma lasers can be further reduced by an order of magnitude, which can significantly enhance the Purcell factor to higher than 100. Our study revealed that precise fabrication of a nanostructure on single-crystalline quality metals can further reduce SPP lasers to a much smaller volume. In addition, the use of ultrahigh-quality Ag produced through self-assembly reduces the threshold of SPP nanolasers by more than tenfold in comparison with polycrystalline Ag. Studies on quasi-one-dimensional SPP lasers represent a critical milestone for future development in the fields of plasmonics and lasers. The unambiguous demonstration of quasi-one-dimensional SPP lasing in a metal grating structure completes the puzzle of the SPP nanolaser family. In addition, the results pave the way to manipulating optical fields at a deep subwavelength scale, which can be applied to plasmonic quantum information physics, nonlinear, optics, and high-density plasmonic circuits (Fig. 9).

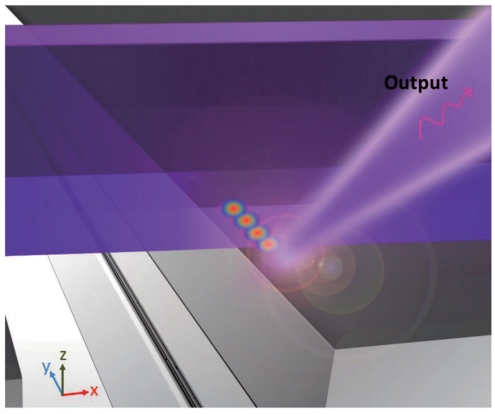


Fig. 8. (color online) Schematic plot of the pseudowedge SPP plasmon laser.

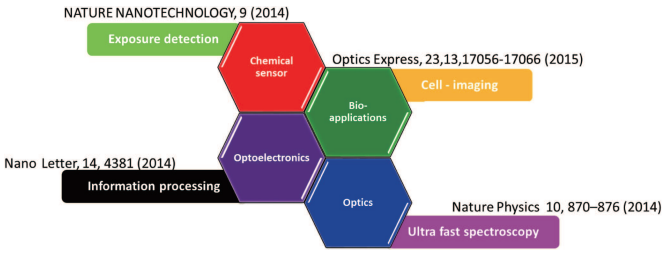


Fig. 9. (color online) Potential applications of SPP nanolasers.[101–105]

6. Conclusions and applications

The increasing demand for smaller, faster, cheaper, and more efficient integrated circuits has led to a rapid development of electronic devices in the past decades. Unlike electrons, photons are neutral and weightless, and they do not interact with each other. Using photons for integrated circuit interconnections to reduce inherent transmission loss and energy consumption between electronic devices is considered the most plausible solution. Within this context, SPP nanolasers have great potential to realize on-chip optical communications that are high-speed, distortion-free, and low-power. The use of an SPP nanolaser is expected to be superior to current electrical transistor-based interconnecting systems, and is expected to greatly improve the performance of integrated circuits. From a practical point of view, SPP nanolasers must be able to be integrated with silicon-based platforms. Among available metals, Al has proven to be compatible with existing CMOS technology.[101–103] Thus, the implementation of Al-based SPP nanolasers is one candidate for sources of on-chip coherent light. Moreover, SPP nanolasers are destined for low output power because of their small size. Hence, in addition to use as on-chip connections, other applications of SPP nanolasers mainly focus on their interaction with the microscopic world. Because of their small footprint and low power output, SPP nanolasers can be used for biomedical purposes. SPP nanolasers are sensitive to changes in the ambient refractive index, which implies that they can be used for cell, virus, or harmful substance detection.[104,105] Furthermore, the size of SPP nanolasers is comparable to that of virus or cancer cells. A designed SPP nanolaser with the correct wavelength would be useful for virus diagnostics or even killing cancerous tissues.[106] By studying SPP nanolaser technology, researchers might be able to further develop various novel applications.

Acknowledgment

Authors acknowledge the help of Profs. S. D. Lin, K. P. Chen at “National” Chiao Tung University and Prof. S. Gwo at “National” Tsing Hua University.

References

[1] Maiman T H 1960 *Nature* **187** 493
[2] Hall R N, Fenner G E, Kingsley J D, Soltys T J and Carlson R O 1962 *Phys. Rev. Lett.* **9** 366

[3] Okuda H, Soda H, Moriki K, Motegi Y and Iga K 1979 *Jpn. J. Appl. Phys.* **18** 2393

[4] Albert F, Braun T, Heindel T, Schneider C, Reitzensteina S, Höfling S, Worschech L and Forchel A 2010 *Appl. Phys. Lett.* **97** 101108

[5] Sandoghdar V, Treussart F, Hare J, Lefèvre-Seguin V, Raimond J M and Haroche S 1996 *Phys. Rev. A* **54** R1777

[6] Noda S 2006 *Science* **314** 260

[7] Eaton S W, Fu A, Wong A B, Ning C Z and Yang P 2016 *Nat. Rev. Mater.* **1** 16028

[8] Hill M T, Oei Y S, Smalbrugge B, Zhu Y, DeVries T, Van Veldhoven P J, Van Otten F W M, Eijkemans T J, Turkiewicz J P and De Waardt H 2007 *Nat. Photon.* **1** 589

[9] Nezhad M P, Simic A, Bondarenko O, Slutsky B, Mizrahi A, Feng L A, Lomakin V and Fainman Y 2010 *Nat. Photon.* **4** 395

[10] Ding K, Liu Z C, Yin L J, Hill M T, Marell M J H, van Veldhoven P J, Noetzel R and Ning C Z 2012 *Phys. Rev. B* **85** 041301

[11] Khajavikhan M, Simic A, Katz M, Lee J H, Slutsky B, Mizrahi A, Lomakin V and Fainman Y 2012 *Nature* **482** 204

[12] Y u K, Lakhani A and Wu M C 2010 *Opt. Express* **18** 8790

[13] Ding K, Hill M T, Liu Z C, Yin L J, van Veldhoven P J and Ning C Z 2013 *Opt. Express* **21** 4728

[14] Bergman D J and Stockman M I 2003 *Phys. Rev. Lett.* **90** 027402

[15] Stockman M I 2008 *Nat. Photon.* **2** 327

[16] Stockman M I 2010 *J. Opt.* **12** 024004

[17] Noginov M A, Zhu G, Belgrave A M, Bakker R, Shalaev V M, Narimanov E E, Stout S, Herz E, Suteewong T and Wiesner U 2009 *Nature* **460** 1110

[18] Premaratne M and Stockman M I 2016 *Adv. Opt. Photon.* **9** 81

[19] Hill M T 2009 *Opt. Express* **17** 11110

[20] Oulton R F, Sorger V J, Zentgraf T, Ma R M, Gladden C, Dai L, Bartal G and Zhang X 2009 *Nature* **461** 629

[21] Lu Y et al 2012 *Science* **337** 450

[22] Lu Y J et al 2014 *Nano Lett.* **14** 4381

[23] Purcell E M 1946 *Phys. Rev.* **69** 681

[24] G´erard J, Sermage B, Gayral B, Legr, B, Costard E and Thierry-Mieg V 1998 *Phys. Rev. Lett.* **81** 1110

[25] Gayral B, Gerard J M, Lematre A, Dupuis C, Manin L and Pelouard J L 1999 *Appl. Phys. Lett.* **75** 1908

[26] Song B S, Noda S, Asano T and Akahane Y 2005 *Nat. Mater.* **4** 207

[27] Vernooy D W, Ilchenko V S, Mabuchi H, Streed E W and Kimble H J 1998 *Opt. Lett.* **23** 247

[28] Yablonovitch E 1987 *Phys. Rev. Lett.* **58** 2059

[29] Painter O, Lee R K, Scherer A, Yariv A, O'Brien J D, Dapkus P D and Kim I 1999 *Science* **284** 1819

[30] Park H G, Kim S H, Kwon S H, Ju Y G, Yang J K, Baek J H, Kim S B and Lee Y H 2004 *Science* **305** 1444

[31] Altug H, Englund D and Vuckovic J 2006 *Nat. Phys.* **2** 484

[32] Nozaki K, Kita S and Baba T 2007 *Opt. Express* **15** 7506

[33] Tandaechanurat A, Ishida S, Guimard D, Nomura M, Iwamoto S and Arakawa Y 2011 *Nat. Photon.* **5** 91

[34] Strauf S and Jahnke F 2011 *Photon. Rev.* **5** 607

[35] Imada M, Noda S, Chutinan A and Tokuda T 1999 *Appl. Phys. Lett.* **75** 316

[36] Imada M, Chutinan A, Noda S and Mochizuki M 2002 *Phys. Rev. B* **65** 195306

[37] Lu T C, Chen S W, Lin L F, Kao T T, Kao C C, Yu P, Kuo H C, Wang S C and Fan S 2008 *Appl. Phys. Lett.* **92** 011129

[38] Lu T C, Chen S W, Kao T T and Liu T W 2008 *Appl. Phys. Lett.* **93** 111111

[39] Chen S W, Lu T C and Kao T T 2009 *IEEE JSTQE* **15** 885

[40] Chen S W, Lu T C, Hou Y J, Liu T C, Kuo H C and Wang S C 2010 *Appl. Phys. Lett.* **96** 071108

[41] Weng P H, Wu T T, Lu T C and Wang S C 2011 *Opt. Lett.* **36** 1908

[42] Pan C H, Lin C H, Chang T Y, Lu T C and Lee C P 2015 *Opt. Express* **23** 11741

[43] Hong K B, Yang C C and Lu T C 2016 *IEEE JQE* **52** 6400205

[44] Huang S C, Hong K B, Chiu H L, Lan S W, Chang T C, Li H and Lu T C 2018 *Appl. Phys. Lett.* **112** 061105

[45] Huang M H, Mao S, Feick H, Yan H Q, Wu Y Y, Kind H, Weber E, Russo R and Yang P D 2001 *Science* **292** 1897

[46] Dasgupta N P, Sun J W, Liu C, Brittman S, Andrews S C, Lim J, Gao H W, Yan R X and Yang P D 2014 *Adv. Mater.* **26** 2137

[47] Maier S A 2006 *Opt. Commun.* **258** 295

[48] Wood R W 1902 *Philos. Mag.* **4** 396

[49] Fano U 1941 *J. Opt. Soc. Am.* **31** 213

[50] Hessel A and Oliner A A 1965 *Appl. Opt.* **4** 1275

[51] Ritchie R H 1957 *Phys. Rev.* **106** 874

[52] Ritchie R H, Arakawa E T, Cowan J J and Hamm R N 1968 *Phys. Rev. Lett.* **21** 1530

[53] Kretschmann E and Raether H 1968 *Z. Naturforsch. A* **23** 2135

[54] Otto A 1968 *Z. Phys.* **216** 410

[55] Li X F and Yu S F 2010 *Opt. Lett.* **35** 2535

[56] Zheludev N I, Prosvirnin S L, Papasimakis N, Fedotov V A 2008 *Nat. Photon.* **2** 351

[57] Flynn R A, Kim C S, Vurgaftman I, Kim M, Meyer J R, Mäkinen A J, Bussmann K, Cheng L, Choa F S and Long J P 2011 *Opt. Express* **19** 8954

[58] Meng X, Kildishev A V, Fujita K, Tanaka K and Shalaev V M 2013 *Nano Lett.* **13** 4106

[59] Ramezani M, Halpin A, Fernández-Domínguez A I, Feist J, Rodriguez S R K, Garcia-Vidal F J and Rivas J G 2017 *Optica* **4** 31

[60] Alam M Z, Aitchison J S and Mojahedi M 2014 *Laser Photon. Rev.* **8** 394

[61] Sidiropoulos T P H, Roder R, Geburt S, Hess O, Maier S A, Ronning C and Oulton R F 2014 *Nat. Phys.* **10** 870

[62] Zhang Q, Li G Y, Liu X F, Qian F, Li Y, Sum T C, Lieber C M and Xiong Q H 2014 *Nat. Commun.* **5** 4953

[63] Chou Y H, Chou B T, Chiang C K, Lai Y Y, Yang C T, Li H, Lin T R and Lu T C 2015 *ACS Nano* **9** 3978

[64] Chou B T, Chou Y H, Wu Y M, Chung Y C, Hsueh W J, Lin S W, Lu T C, Lin T R and Lin S D 2016 *Sci. Rep.* **6** 1

[65] Chou Y H, Wu Y M, Hong, K B Chou B T Shih J H, Chung Y C Chen P J, Lin T R, Lin C C, Lin S D and Lu T C *Nano Lett.* **16** 3179

[66] Fox M 2010 *Optical Properties of Solids* (Oxford: Oxford University Press)

[67] Drude P 1900 *Ann. Phys.* **306** 566

[68] Naik G V, Shalaev G M and Boltasseva A 2013 *Adv. Mater.* **25** 3264

[69] Khurgin J B and Boltasseva A 2012 *MRS Bull.* **37** 768

[70] West P R, Ishii S, Naik G V, Emani N K, Shalaev V M and Boltasseva A 2010 *Laser Photon. Rev.* **4** 795

[71] Chung Y C, Cheng P J, Chou Y H, Chou B T, Hong K B, Shih J H, Lin S D, Lu T C and Lin T R 2017 *Sci. Rep.* **7** 39813

[72] Kazmerski L and Racine D M 1975 *J. Appl. Phys.* **46** 791

[73] Clegg P 1952 *Proc. Phys. Soc. Lond. Sect. B* **65** 774

[74] Denier van derGon A, Tromp R and Reuter M 1993 *Thin Solid Films* **236** 140

[75] Park K H, Ha J S and Lee E H 1997 *ETRI J.* **19** 71

[76] Logeeswaran V, Chan M L, Bayam Y, Saif Islam M, Horsley D, Li X, Wu W, Wang S and Williams R 2007 *Appl. Phys. A* **87** 187

[77] Chen W, Thoreson M D, Ishii S, Kildishev A V and Shalaev V M 2010 *Opt. Express* **18** 5124

[78] Pashley D 1959 *Philos. Mag.* **4** 316

[79] Palmberg P, Rhodin T and Todd C 1967 *Appl. Phys. Lett.* **11** 33

[80] Nagpal P, Lindquist N C, Oh S H and Norris D J 2009 *Science* **325** 594

[81] Boltasseva A and Atwater H A 2011 *Science* **331** 290

[82] Park J H, Ambwani P, Manno M, Lindquist N C, Nagpal P, Oh S H, Leighton C and Norris D J 2012 *Adv. Mater.* **24** 3988

[83] Wu Y W, *et al.* 2014 *Adv. Mater.* **26** 6106

[84] Wang C Y, Chen H Y, Sun L, Chen W L, Chang Y M, Ahn H, Li X and Gwo S 2015 *Nat. Commun.* **6** 7734

[85] Chou Y H, Hong K B, Chang C T, Chang T C, Huang Z T, Cheng P J, Yang J H, Lin M H, Lin T R, Chen K P, Gwo S and Lu T C 2018 *Nano Lett.* **18** 747

[86] Berini P and De Leon I 2012 *Nat. Photon.* **6** 16

[87] Gwo S and Shih C K 2016 *Rep. Prog. Phys.* **79** 086501

[88] Ozgur U, Alivov Y I, Liu C, Teke A, Reshchikov M A, Dogan S, Avrutin V, Cho S J and Morkoc H 2005 *J. Appl. Phys.* **98** 041301

[89] Wang S, Wang X Y, Li B, Chen H Z, Wang Y L, Dai L, Oulton R F and Ma R M 2017 *Nat. Commun.* **8** 1889

[90] Kao T S, Chou Y H, Chou C H, Chen F C and Lu T C 2014 *Appl. Phys. Lett.* **105** 231108
[91] Kao T S, Hong K B, Chou Y H, Huang J F, Chen F C and Lu T C 2016 *Opt. Express* **24** 20696
[92] Zhu H, Fu Y, Meng F, Wu X, Gong Z, Ding Q, Gustafsson M V, Trinh M T, Jin S and Zhu X Y 2015 *Nat. Mater.* **14** 636
[93] Xing G, Mathews N, Lim S S, Yantara N, Liu X, Sabba D, Grätzel M, Mhaisalkar S and Sum T C 2014 *Nat. Mater.* **13** 476
[94] Chang S W, Lin T R and Chuang S L 2010 *Opt. Express* **18** 15039
[95] Pitarke J M, Silkin V M, Chulkov E V and Echenique P M 2007 *Rep. Prog. Phys.* **70** 1
[96] Barnes W L, Dereux A and Ebbesen T W 2003 *Nature* **424** 824
[97] Schuller J A, Barnard E S, Cai W, Jun Y C, White J S and Brongersma M L 2010 *Nat. Mater.* **9** 193
[98] Stockman M I 2011 *Opt. Express* **19** 22029
[99] Novotny L and Hecht B 2012 *Principles of Nano-Optics* (2nd Edn.) (Cambridge: Cambridge University Press)
[100] Chou Y H, Hong K B, Chung Y C, Chang C T, Chou B T, Lin T R, Arakelian S M, Alodjants A P and Lu T C 2017 *IEEE JSTQE* **23** 4601907
[101] Chou B T, Lu T C and Lin S D 2015 *J. Lightw. Technol.* **1** 1
[102] Neira A D, Wurtz G A, Ginzburg P and Zayats A V 2014 *Opt. Express* **22** 10987
[103] Pavarelli N et al 2015 *J. Light. Technol.* **33** 991
[104] Ma R M, Ota S, Li Y M, Yang S and Zhang X 2014 *Nat. Nanotechnol.* **9** 600
[105] Abe H, Narimatsu M, Watanabe T, Furumoto T, Yokouchi Y, Nishijima Y, Kita S, Tomitaka A, Ota S, Takemura Y and Toshihiko Baba 2015 *Opt. Express* **23** 17056
[106] Atwater H A 2007 *Sci. Am.* **296** 56